

Structural, Magnetic and Magneto-Optical Properties of Substituted Ba Ferrite Films Grown by RF Sputtering

J. K. Cho

*Department of Electrical and Computer Engineering, Carnegie Mellon University,
Pittsburgh, Pennsylvania 15213, USA*

(Received 3 January 1992)

Structural, magnetic and magneto-optical(1.0~3.2eV) properties of rare earth(Ce, Pr, Eu), transition metal(Ni, Co), and Al substituted polycrystalline Ba ferrite films grown by rf sputtering have been investigated. TEM studies revealed that crystal grains in the films were reduced in size from several hundred nm to the order of 1 nm with the decrease of rf power density during sputtering. By substituting Al, square hysteresis loops have successfully been obtained. It has been found that Ni ions strongly enhances Faraday rotation of the films in the visible range. It has been confirmed that Co ions also strongly enhances Faraday rotation of the films in the near infrared. Enhancement in Faraday rotation by Ce, Pr, and Eu ions has not been observed. The origin of the enhancement in magnetic and magneto-optical properties of the films is discussed.

I. Introduction

Magneto-optical(MO) memory has attracted attention as a reliable high density erasable data storage system for computer and communication systems. In MO memory, by utilizing the fact that light can be focused using lenses, sufficient distance between head and media has been successfully achieved without deteriorating recording density, which is generally difficult in competitive magnetic memory based on electromagnetic induction. Because it is relatively easy to prepare optically homogeneous films having magnetization perpendicular to the film plane, amorphous rare earth transition metal alloy a-RT(e.g. TbFeCo) films have been used as MO memory media. The films, however, have MO figure of merit ($R\theta_k$ for media using Kerr rotation and $2F\exp(-2\alpha h)$ for media using Faraday effect, where R is refractivity and θ_k Kerr rotation angle, F Faraday rotation angle per unit length, h thickness of film, and α absorption

coefficient) as low as 0.25 deg and are easy to oxidize due to rare earth element[1].

To overcome the shortcomings of the a-RT films and to increase recording density by using shorter wavelength laser in the future, transition-metal noble metal ultra thin multilayers (e.g. Co/Pt) and oxide films have been studied. Of these, Co/Pt films have overcome some of the drawback of the a-RT, such as the deterioration of the figure of merit in shorter wavelengths and problems due to oxidation, but the films show figure of merit still as low as 0.4 deg[2].

The oxide films have feature that the figure of merit of the films can be increased using the ions which enhance MO effect, such as Bi^{3+} , Pb^{2+} , Ce^{3+} , Pr^{3+} , and Co^{2+} [3~6]. For instance, Bi substituted iron garnet ($\text{RBi})_3\text{Fe}_5\text{O}_{12}$ (Bi:RIG) films have figure of merit one or two orders higher than those of the above metal films[6]. The oxide films have high intrinsic corrosion resistance as well. The films, however, generally have a problem of high media noise due to light scattering

scattering at grain boundaries, since they are prepared only in polycrystalline form on most of substrates except single crystal wafers having compatible structure. However, this approach is not economically attractive[7]. Ba ferrite $BaFe_{12}O_{19}$ films studied in this work have figure of merit lower than that of Bi:RIG films but higher than the metal films in near infrared [8] and hysteresis loops which are not satisfactorily square for MO memory[9]. The films, however, have strong magnetocrystalline anisotropy which results in smaller minimum domain diameter $d_{min}(d_{min} \sigma_w / 2M_s H_c$, where σ_w is domain wall energy density, M_s saturation magnetization, and H_c coercivity) and higher potential recording density. Thus if we find proper ions which enhance the figure of merit and squareness, and establish techniques allowing optically homogeneous films with fine crystal grains, the films will be excellent candidates for high density MO memory media in the future.

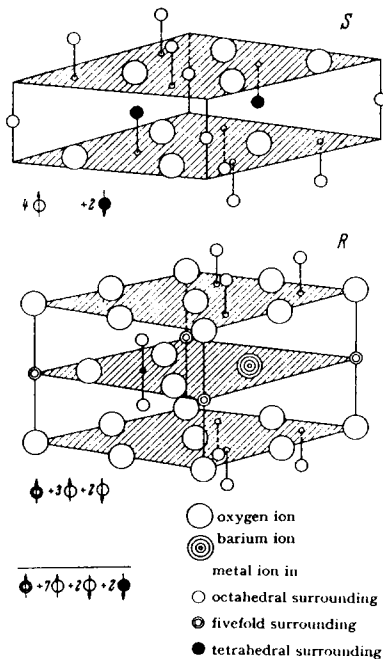


Fig.1. Structure of Ba ferrite $BaFe_{12}O_{19}$. The unit cell includes the blocks $RSR^*S^*R^*$ and S^* are the blocks obtained by a respective rotation of R and S blocks over an angle of 180 degree around the c axis.

Ba ferrite is a hexagonal ferrimagnetic material having a space group $P6_3/mmc(D_{6h}^4)$. There are one Ba^{2+} and twelve Fe^{3+} ions in a unit cell. Nine Fe ions occupy octahedral sites; of these, seven have up spins and two have down spins. Two Fe ions having down spins occupy tetrahedral sites. The last one having a up spin fits to a fivefold surrounding(Fig.1). The crystal structure is characterized by repeating two blocks; one(S block) includes only Fe ions(octahedral and tetrahedral) and the other (R block) includes both Ba and Fe(octahedral and fivefold) ions[10].

Kahn measured ultraviolet Kerr rotation spectra on bulk Ba ferrite single crystals and assigned observed peaks to charge transfer transitions of 2p electrons of O^{2-} ions to 3d orbits of octahedrally (4.43 eV) and tetrahedrally(5.5 eV) coordinated Fe ions [11]. Shono et al. measured infrared Faraday rotation and absorption spectra on bulk single crystals and reported the figure of merit of them[8]. Machida et al. found that Co ions enhanced MO effect in the near infrared[12]. Nakamura et al., however, found that the squareness of sputtered Co-Ti substituted polycrystalline Ba ferrite films was rapidly reduced due to the decrease of magnetocrystalline anisotropy as Co concentration increased[9]. Kaneko et al. obtained the signal to noise ratio of 50 dB at 800 nm and 30-kHz bandwidth using the films[13].

In this study, we investigated Faraday rotation spectra of rare earth(Ce, Pr, and Eu) and transition metal(Ni, Co) substituted Ba ferrite films to find the MO effect enhancing ions. We also investigated magnetic properties of Al substituted films to obtain square hysteresis loops. We tried to reduce crystal grain size of Ba ferrite films by changing parameters of sputtering.

II. Film Preparation

Polycrystalline films $0.4 \sim 1 \mu m$ thick of $Ba_{1-x}R_xFe_{12-x}M_xO_{19}$ ($R=La, Ce, Pr, M=Ni, Co, x=0 \sim 0.8$), $Ba_{1-x}Eu_xFe_{12}O_{19}$ ($x=0 \sim 4.0$) were grown using rf sputtering technique, Table I summarizes the parameters of sputtering. Sintered ceramic discs(70 mm ϕ) were

used as targets. Silica glass and $Gd_3Ga_5O_{12}$ single crystal wafers ($20 \times 20 \times 0.5 \text{ mm}^3$) were used as substrates. The single crystal wafers which had closer thermal expansion coefficient to that of the films were necessary to grow crack-free films. Substrate temperature, T_s , was maintained at $400 \sim 600^\circ\text{C}$ during sputtering. rf power density, PD_{rf} , was varied in the range of $6 \sim 24 \text{ W/cm}^2$.

Table I. Parameters of Sputtering

target	ceramic discs; $Ba_{1-33(1+x)}R_xFe_{12-x}M_{1.5(1-x)}O_{19}$, (R = La, Pr, M = Ni, Co, x = 0, 0.3, 0.6) $Ba_{1-x}Ce_xFe_{12-x}Ni_xO_{19}$, (x = 0, 0.3, 0.6) $Ba_{1-x}Ce_xFe_{12}Ni_xO_{19}$, (x = 0, 3, 4) $BaFe_{12-x}Al_xO_{19}$, (x = 0, 3, 4)
sputtering gas	pure Ar or mixed gas of Ar:O ₂ = 9:1
pressure	50 m Torr
rf power density	$6 \sim 24 \text{ W/cm}^2$
deposition rate	$7 \sim 20 \text{ nm/min}$
substrate	silica glass or (111) oriented $Gd_3Ga_5O_{12}$ single crystal wafer
substrate temp	$400 \sim 600^\circ\text{C}$

We tried to control crystal grain size in the films by varying PD_{rf} . Increase in PD_{rf} accelerated sputtering gas, increases kinetic energy of sputtered particles knocked out from the target, and increases mobility of the particles on the surface of the substrate.

Pure Ar gas was used for preparation of Ce and Eu substituted films to incorporate them as Ce^{3+} and Eu^{2+} , avoiding Ce^{4+} and Eu^{3+} which are more stable under an oxidizing atmosphere; it is known that the latter do not enhance MO effect in iron garnets[3]. Mixed gas of Ar:O₂=9:1 was used for other films.

III. Results and Discussion

1. Chemical composition

Table II shows chemical composition of the films deposited at $T_s=550^\circ\text{C}$ and $PD_{rf}=20 \text{ W/cm}^2$. The

films obtained were nearly stoichiometric. Table III shows chemical composition of the films deposited at different PD_{rf} . The chemical composition of the films did not change much with PD_{rf} .

Table II. Chemical composition of two films grown at $T_s=550^\circ\text{C}$ and $PD_{rf}=20 \text{ W/cm}^2$

number	atomic ratio							
	Ba	La	Ce	Pr	Eu	Fe	Ni	Co
1	1.08	—	—	—	—	12.00	—	—
2	0.64	0.30	—	—	—	11.70	0.37	—
3	0.71	0.28	—	—	—	11.70	—	0.36
4	0.86	—	0.37	—	—	11.70	0.26	—
5	0.71	—	—	0.30	—	11.70	0.38	—
6	0.78	—	—	—	0.31	12.00	—	—

Table III. Chemical composition of two films grown at $T_s=550^\circ\text{C}$ and Different PD_{rf} .

number	rf power density (W/cm^2)	atomic ratio			
		Ba	La	Fe	Co
3	20	0.71	0.28	11.70	0.36
7	9	0.77	0.29	11.70	0.38

2. Structure

The films deposited at $PD_{rf} < 13 \text{ W/cm}^2$ and $T_s < 570^\circ\text{C}$ showed no x-ray diffraction lines due to crystal phases, as shown in Fig.2. The films deposited at $PD_{rf} > 19 \text{ W/cm}^2$ and $T_s > 550^\circ\text{C}$ showed diffraction lines due to preferential crystal orientation that the basal planes {001} of Ba ferrite parallel to the film plane. Similar results were obtained for the substituted films.

Figure 3 shows c axis lattice constant of representative $Ba_{1-x}La_xFe_{12-x}Co_xO_{19}$ films. The lattice constant (23.23 Å) obtained for Ba ferrite films (x=0) agrees well with bulk value (23.2 Å)[10]. The lattice constant of the substituted films linearly decreases as x increases. From ionic radii ($Ba^{2+}:1.38 \text{ Å}$, $La^{3+}:1.15 \text{ Å}$, $Fe^{3+}:0.67 \text{ Å}$, $Co^{2+}:0.78 \text{ Å}$ [10]), La and Co ions are considered to substitute for Ba and Fe ions,

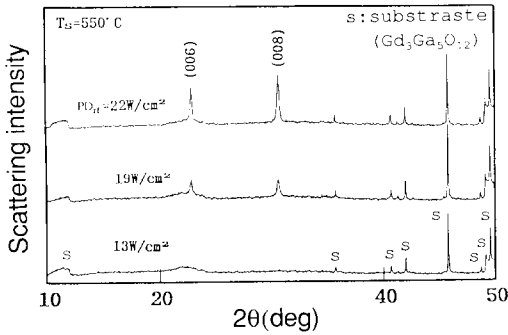


Fig. 2. X-ray diffraction patterns of the films deposited at $T_s=550^\circ\text{C}$ and various PD_{rf} .

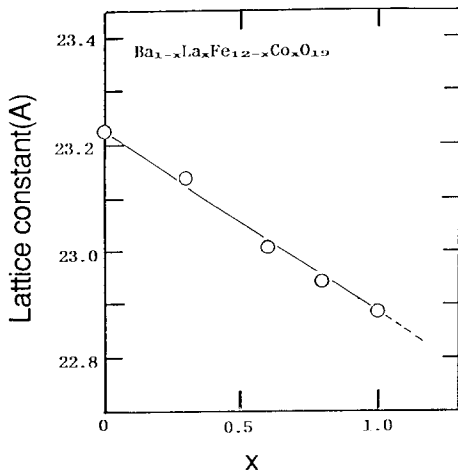


Fig. 3. Dependence of c axis lattice constant on x in $\text{Ba}_{1-x}\text{La}_x\text{Fe}_{12-x}\text{Co}_x\text{O}_{19}$ films. The lattice constants are calculated using (008) diffraction lines.

respectively.

Figure 4 shows morphology of the films. The films deposited at lower PD_{rf} have columnar-like structure. The films deposited at higher PD_{rf} are more smooth and denser.

Figure 5 shows TEM images and selected area electron diffraction patterns of the films. Grains of the order of 100 nm in diameter are seen in the bright field image (a) of the films deposited at $PD_{rf}=22$ W/cm^2 . Groups of spots due to grains with different

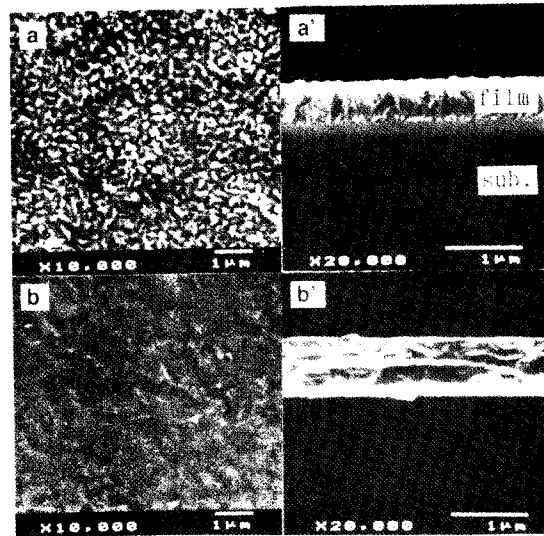


Fig. 4. Secondary electron SEM images of surface (a, b) and cross section (a', b') of the films deposited at $PD_{rf}=9$ (a, a') and 20 W/cm^2 (b, b').

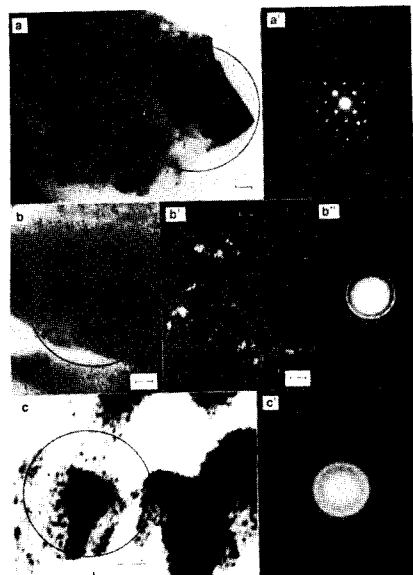


Fig. 5. Bright (a, b, c) and dark (b', c') field TEM images and selective area diffraction patterns (a', b', c') of the films deposited at $PD_{rf}=22$ (a, a'), 19 (b, b'), and 9 W/cm^2 (c, c'). The scales represent 50 nm.

crystal orientation are seen in the selected area (within the circle including a few grains) diffraction patterns (a'). This implies that the films may have crystal grains of the order of 100 nm. In the films deposited at 19 W/cm^2 , grains of the order of 10 nm are seen in bright (b) a and dark (b' , contrast based on electron diffraction) field images. Rings are seen in selected area (within the circle including a lot of the grains) diffraction patterns. The films, therefore, may have crystal grains of the order of 10 nm. In the films deposited at $PD_{rf}=9 \text{ W/cm}^2$, grains are not clearly distinguished in bright field image (c). Rings and a halo are observed in selected area diffraction patterns(c'). Considering the films showed no x-ray diffraction lines (Fig. 2), as mentioned above, the films may be composed of crystal grains of the order of 1 nm and amorphous phase.

3. Magnetic properties

Figure 6 shows magnetization M_s , coercivity H_c and squareness ratio R_s of substituted films. M_s increases with the increase of PD_{rf} and reaches a constant value(330 emu/cm^3) at $PD_{rf} > 15 \text{ W/cm}^2$, which

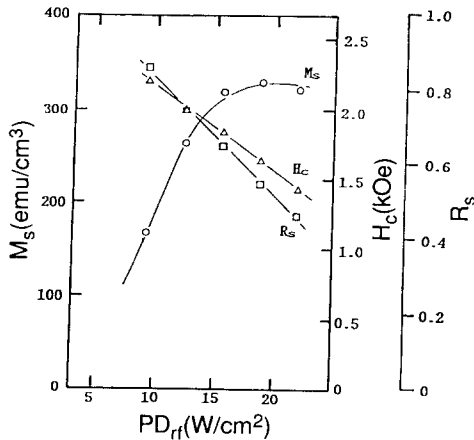


Fig. 6. Dependence of saturation magnetization, coercivity, and squareness ratio on PD_{rf} in $\text{Ba}_{1-x}\text{Pr}_x\text{Fe}_{12-x}\text{Ni}_x\text{O}_{19}$ ($x=0.35$) films.

agrees with bulk value(335 emu/cm^3 [10]) within experimental error. Lower M_s in the films deposited at lower PD_{rf} may be ascribed to the amorphous phase

as observed by the above TEM studies. On the other hand, H_c and M_s decrease with the increase of PD_{rf} . This may be due to grain growth during sputtering. Figure 7 compares perpendicular hysteresis loops of Ba ferrite and Al substituted Ba ferrite films. The latter shows squareness ratio of unit and higher H_c . Kondo et al. reported that magnetocrystalline anisotropy of Ba ferrite is originated from fivefold Fe ions [14, 15]. Bitetto et al found that M_s decreases rapidly but the anisotropy decreases slowly by a factor of 2 with increasing Al concentration in bulk Ba ferrites and suggested that Al ions may selectively substitute for octahedral Fe ions having up spins[16]. This may explain the results obtained in the present study.

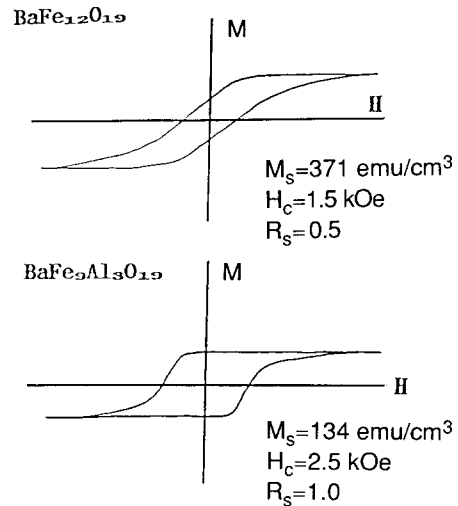


Fig. 7. Magnetic hysteresis loops of Ba ferrite and Al substituted Ba ferrite films. The loops are traced by a vibrating sample magnetometer.

4. Magneto-optical properties

The shape of Faraday rotation spectra of the films did not qualitatively depend on PD_{rf} . The only quantitatively depended on M_s values of the films.

Figure 8 shows Faraday rotation spectra of Ba ferrite and Al substituted Ba ferrite films. Structure at $h\nu < 2.5 \text{ eV}$ qualitatively agrees with that of Nakamura et al[9]. New peaks are found at $h\nu > 2.5 \text{ eV}$. Of these, the peak at 2.63 eV shows Faraday rotation as large as $2 \times 10^4 \text{ deg/cm}$. By Al substitution,

Faraday rotation generally decreases except the peak at ~ 3.0 eV. This may be ascribed to the selective substitution of Al ions for Fe ions in certain sites.

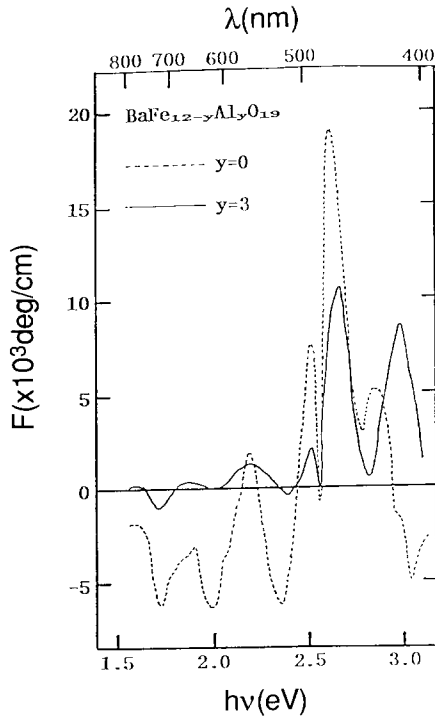


Fig. 8. Faraday rotation spectra of Ba ferrite and Al substituted Ba ferrite films. The spectra were measured by polarization modulation method using a monochromator combined with halogen and xenon lamps.

It was also found that Ni ions enhanced Faraday rotation of the films in the visible range as shown in Fig. 9. La ions are substituted for charge compensation. Ni²⁺ ions have been expected to enhance MO effect. But because ferromagnetic materials having high concentration of Ni²⁺ have not been found so far, the contribution of the ions on MO effect have been studied using nonmagnetic materials doped with the ions. Weaklim measured absorption spectra of Ni²⁺ doped ZnO and concluded that the crystal field transition of 3d electrons of tetrahedrally coordinated Ni²⁺ ions occur at 0.57 eV (${}^3T_1(F) \rightarrow {}^3T_2(F)$), 1.03

eV (${}^3T_1(F) \rightarrow {}^3A_2(F)$), and 2.00 eV (${}^3T_1(F) \rightarrow {}^3T_1(P)$) [17]. But those lack in higher energy data and do not agree with the spectra obtained in the present study.

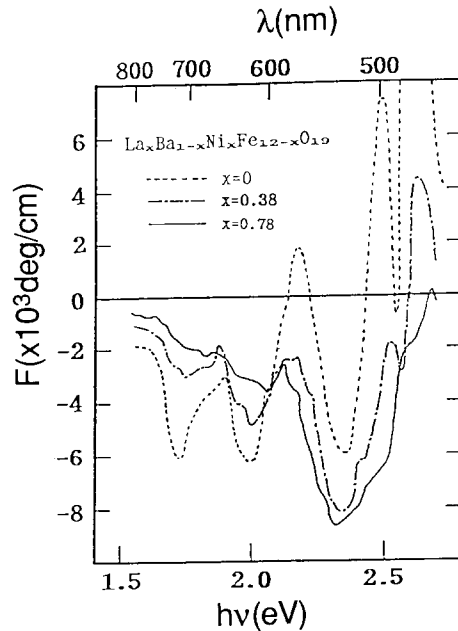


Fig. 9. Faraday rotation spectra of Ni substituted Ba ferrite films.

Figure 10 shows Faraday rotation spectra of Co substituted films. The spectra agree qualitatively with those of Nakamura et al. it was confirmed, thus, that Co ions enhance Faraday rotation in the near infrared. The contribution of Co ions in Ba ferrites may be explained, like in iron garnets, as follows. Because Co²⁺ ions occupy tetrahedral sites and they do not have centrosymmetry, 3d orbits of them couple with 2p orbits of O²⁻. This makes the crystal field transitions (1.2 eV ; ${}^4A_2(F) \rightarrow {}^4T_1(F)$ and 1.8 eV ; ${}^4A_2(F) \rightarrow {}^4T_1(P)$) of the 3d electrons, which are originally forbidden, parity-allowed, which results in strong oscillator strength [17]. The dispersive transition centered at ~ 1.8 eV observed in the present study may be ascribed to one of the crystal field transitions. However, further studies are needed, to clarify the contribution of Co ions at higher energy. Enhancement in Faraday rotation was not observed in Ce, Pr, and Eu substituted films in this study.

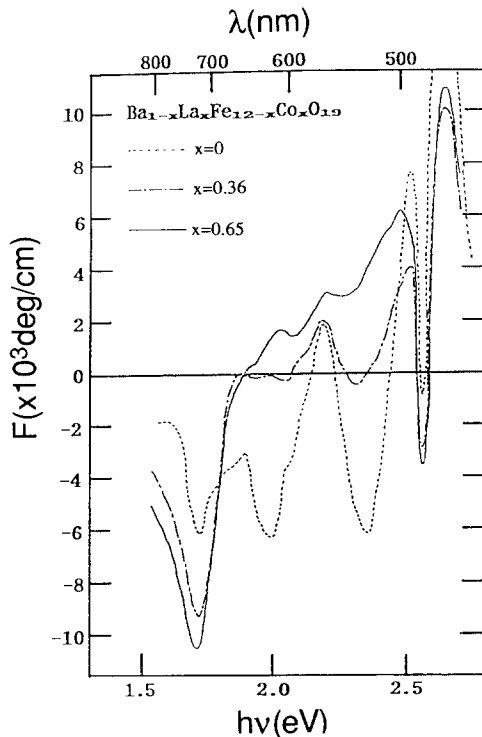


Fig. 10. Faraday rotation spectra of Co substituted Ba ferrite films.

It is surprising that Pr ions do not enhance Faraday rotation in Ba ferrites. The ions have been expected to enhance Faraday rotation in Ba ferrites, as in garnets, since the enhancement by the ions in garnet have been considered to be based on internal transitions $4f \rightarrow 5d$ of Pr^{3+} , according to Hansen et al., it is ascribed to the large spin orbit splitting in excited 5d state generated by the allowed internal transitions[4].

IV. Conclusions

It has been demonstrated that the crystal grains in Ba ferrite films can be successfully reduced in size up to order of 1nm by decreasing rf power density during sputtering. By substituting Al ions, square hysteresis loops has been obtained. A new peak showing rotation as strong as 2×10^4 deg/cm has been

found at visible Faraday rotation spectra of Ba ferrite films. It also has been found that Ni ions strongly enhance Faraday rotation of the films in the visible range. It has been confirmed that Co ions also strongly enhance Faraday rotation in the near infrared. Enhancement of Faraday rotation by Ce, Pr, and Eu ions has not been observed. The Ni(Co), Al substituted Ba ferrite films may have high potential for high density MO memory media in the future.

Acknowledgements

The author would like to thank Dr. M. Gomi for fruitful discussion and Mr. K. Shimai for sample preparation.

References

- [1] K. Sato and Y. Togami, *J. Magn. Magn. Mater.* **35**, 181(1983).
- [2] W. B. Zepper and F. J. A. M. Greidanus, *J. Appl. Phys.* **65**, 497(1989).
- [3] M. Gomi, K. Sato and M. Abe, *Pro. ICF 5*, India, 919(1989).
- [4] P. Hansen, C.-P. Klages and K. Witter, *J. Appl. Phys.* **60**, 721(1986).
- [5] K. Egashira and T. Manabe, *IEEE Trans. Magn. MAG-8*, 646(1973).
- [6] P. Hansen and J.-P. Krumme, *Thin Solid Films*, **114**, 69(1984).
- [7] J. Cho, M. Gomi and M. Abe, *J. Appl. Phys.* **70** (1991)(to be published).
- [8] K. Shono, M. Abe, M. Gomi and S. Nomura, *Jpn. J. Appl. Phys.* **21**, 1720(1982).
- [9] H. Nakamura, F. Ohmi, Y. Kaneko, Y. Sawada, A. Watada and H. Machida, *J. Appl. Phys.* **61**, 3346(1987).
- [10] K. H. Hellwege, *Landolt-Boernstein*, Vol. **4**, New York(1970) pp 558~569.
- [11] F. J. Kahn, P. S. Pershan and J. P. Remeika, *Phys. Rev.* **186**, 891(1969).
- [12] H. Machida, F. Ohmi, Y. Sawada, Y. Kaneko, A. Watada and H. Nakamura, *J. Magn. Magn. Mater.* 54-57, 1399(1986).
- [13] Y. Kaneko, Y. Sawada, F. Ohmi, I. Miyamoto and A. Wasada, *Jpn. J. Appl. Phys. Suppl.* 26-

4, 23(1987).
 [14] J. Kodo, Prog. Theor. Phys. Kyoto, **23**, 106 (1960).
 [15] A. D. Shchurova, T. M. Perekalina and S. S. Fonton, Soviet Phys. JETP, **31**, 840(1970).
 [16] D. J. De Bitetto, J. Appl. Phys. **35**, 3482(1964).
 [17] H. A. Weaklim, J. Chem. Phys. **36**, 2117(1962).
 [18] J.-P. Krumme, V. Doormann and P. Hansen, J. Appl. Phys. **66**, 4393(1989)

스퍼터법으로 제조한 이온 치환 Ba 웨라이트 박막의 구조 및 자기적, 자기광학적 성질

조재경

카네기 멜론대학 전기 및 컴퓨터공학과

(1992년 1월 3일 받음)

전이 금속(Ni, Co), 희토류(Ce, Pr, Eu) 및 Al이온 치환 Ba 웨라이트박막을 스퍼터법으로 제조하여, 그 구조, 자기적 및 자기광학적 성질(1.0eV-3.2eV)을 조사하였다. 막 제작시의 투입 rf 전력 밀도를 조절하는 것의해, 막 중의 결정립의 크기를 수 100 nm-수 nm로 제어하는데 성공했다. Fe를 Al으로 치환하는 것의해 각형 히스테리시스 루우프를 얻는데 성공했다. Ni이온이 가시역에서 페러데이 회전을 크게 증가시키는 것을 발견했다. Co이온이 근적외선 영역에서 페러데이 회전을 크게 증가시키는것을 확인했다. Ce, Pr, Eu이온에 의한 페러데이 회전의 증가는 관찰되지 않았다. 이들 이온 치환 막의 자기적 및 자기광학적 성질의 기원에 대해 고찰했다.